



Discovery of novel selective PI3K γ inhibitors through combining machine learning-based virtual screening with multiple protein structures and bio-evaluation



Jingyu Zhu^{a,1,*}, Kan Li^{a,1}, Lei Xu^b, Yanfei Cai^a, Yun Chen^a, Xinling Zhao^a, Huazhong Li^c, Gang Huang^{d,*}, Jian Jin^{a,*}

^aSchool of Pharmaceutical Sciences, Jiangnan University, Wuxi, Jiangsu 214122, China

^bInstitute of Bioinformatics and Medical Engineering, School of Electrical and Information Engineering, Jiangsu University of Technology, Changzhou 213001, China

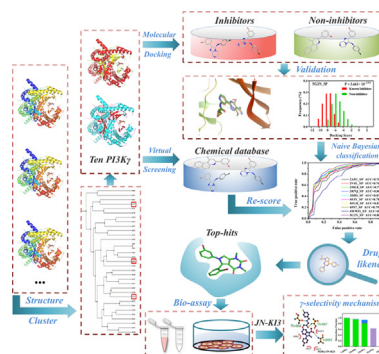
^cSchool of Biotechnology, Jiangnan University, Wuxi, Jiangsu 21412 2, China

^dShanghai Key Laboratory of Molecular Imaging, Shanghai University of Medicine and Health Sciences, Shanghai 201318, China

HIGHLIGHTS

- Virtual screening based on machine learning with multiple proteins was developed.
- Discovery of a novel PI3K γ inhibitor integrating virtual screening and bio-assays.
- JN-KI3 selective inhibit PI3K γ enzymatic activity and hematologic malignancies.
- The selective γ -inhibition mechanism of JN-KI3 was highlighted using MD simulation.

GRAPHICAL ABSTRACT



ARTICLE INFO

Article history:

Received 20 August 2020

Revised 9 April 2021

Accepted 16 April 2021

Available online 20 April 2021

Keywords:

PI3K γ

ABSTRACT

Introduction: Phosphoinositide 3-kinase gamma (PI3K γ) has been regarded as a promising drug target for the treatment of various diseases, and the diverse physiological roles of class I PI3K isoforms (α , β , δ , and γ) highlight the importance of isoform selectivity in the development of PI3K γ inhibitors. However, the high structural conservation among the PI3K family makes it a big challenge to develop selective PI3K γ inhibitors.

Objectives: A novel machine learning-based virtual screening with multiple PI3K γ protein structures was developed to discover novel PI3K γ inhibitors.

Abbreviations: PI3K, Phosphoinositide 3-kinase; RTK, receptor tyrosine kinases; GPCR, G protein-coupled receptors; CADD, computer-aided drug design; VS, virtual screening; MD, molecular dynamics; PDB, protein data bank; RMSD, root-mean-squared-deviation; SP, standard precision; XP, extra precision; DS3.5, discovery studio 3.5; NBC, naive Bayesian classifier; ROC, receiver operations characteristic; AUC, area under receiver operations characteristic curve; REOS, rapid elimination of swill; Badapple, bioactivity data associative promiscuity pattern learning engine; SMILES, simplified molecular input line entry specification; ADMET, absorption, distribution, metabolism, excretion, and toxicity; DMEM, Dulbecco's Modified Eagle Medium; IMDM, Iscove's Modified Dulbecco's Medium; FBS, fetal bovine serum; SD, standard deviation; AKT, protein kinase B; PAGE, polyacrylamide gel electrophoresis; RMSF, root-mean-squared-fluctuation; MM/GBSA, molecular mechanics/generalized born surface area; PAINS, pan-assay interference compounds; PSA, primary screening assays; CDRA, confirmatory dose-response assays; PARP, poly ADP-ribose polymerase; H-bond, hydrogen bond; Ionic, ionic interactions; Water Bridge, hydrogen bonds through water molecular bridge.

Peer review under responsibility of Cairo University.

* Corresponding authors.

E-mail addresses: jingyuzhu@jiangnan.edu.cn (J. Zhu), huanggang@sumhs.edu.cn (G. Huang), jianjin@jiangnan.edu.cn (J. Jin).

¹ Equivalent authors.

<https://doi.org/10.1016/j.jare.2021.04.007>

2090-1232/© 2021 The Authors. Published by Elsevier B.V. on behalf of Cairo University.

This is an open access article under the CC BY license (<http://creativecommons.org/licenses/by/4.0/>).

Selective inhibitor
Hematologic malignancies
Virtual screening
Molecular dynamics simulation
JN-KI3

Methods: A large chemical database was screened using the virtual screening model, the top-ranked compounds were then subjected to a series of bio-evaluations, which led to the discovery of JN-KI3. The selective inhibition mechanism of JN-KI3 against PI3K γ was uncovered by a theoretical study.

Results: 49 hits were identified through virtual screening, and the cell-free enzymatic studies found that JN-KI3 selectively inhibited PI3K γ at a concentration as low as 3,873 nM but had no inhibitory effect on Class IA PI3Ks, leading to the selective cytotoxicity on hematologic cancer cells. Meanwhile, JN-KI3 potentially blocked the PI3K signaling, finally led to distinct apoptosis of hematologic cell lines at a low concentration. Lastly, the key residues of PI3K γ and the structural characteristics of JN-KI3, which both would influence γ isoform-selective inhibition, were highlighted by systematic theoretical studies.

Conclusion: The developed virtual screening model strongly manifests the robustness to find novel PI3K γ inhibitors. JN-KI3 displays a specific cytotoxicity on hematologic tumor cells, and significantly promotes apoptosis associated with the inhibition of the PI3K signaling, which depicts PI3K γ as a potential target for the hematologic tumor therapy. The theoretical results reveal that those key residues interacting with JN-KI3 are less common compared to most of the reported PI3K γ inhibitors, indicating that JN-KI3 has novel structural characteristics as a selective PI3K γ inhibitor.

© 2021 The Authors. Published by Elsevier B.V. on behalf of Cairo University. This is an open access article under the CC BY license (<http://creativecommons.org/licenses/by/4.0/>).

Introduction

The extensive research conducted over the past decades has implicated the role of various cell signaling events in numerous malignant, inflammatory, autoimmune, and cardiovascular diseases, out of which the phosphoinositide 3-kinase (PI3K) signaling is one of the most relevant pathways because of its various vital functions, such as cell survival, proliferation, differentiation, and motility [1]. PI3Ks belong to a family of lipid kinases which catalyze the phosphorylation of the inositol ring of phosphoinositide and then transduce the signals as secondary messengers [2]. PI3Ks are divided into three different classes (I, II, and III) based on their primary structures and the preference of substrates [3]. Comparing to the other two classes, class I PI3Ks have been extensively and exhaustively studied. Class I PI3Ks are consist of two different subclasses, class IA and class IB, according to their signaling pathways and regulating proteins [4]. There are three PI3K isoforms, PI3K α , PI3K β , and PI3K δ , belonging to class IA, and PI3K γ is the only member of class IB. Class IA are activated by receptor tyrosine kinases (RTKs) and other tyrosine kinase coupled receptors [5–7], while class IB accepts the signaling from G protein-coupled receptors (GPCRs) through the interaction between PI3K γ regulatory subunit and the β -subunits of GPCRs [8–10]. A large amount of research has proved that the Class I PI3Ks play multiple crucial roles in a wide variety of cellular processes [11–13], and that makes PI3K as a promising drug target for the treatment of cancers, inflammations, and immune disorders [3–7]. Nowadays, four PI3K inhibitors have been pushed into the market, namely, Idelalisib in 2014 (PI3K δ inhibitor) [14,15], Copanlisib in 2017 (pan-PI3K inhibitor) [16], Duvelisib in 2018 (PI3K δ/γ dual inhibitor) [17] and Alpelisib in 2019 (PI3K α inhibitor) [18,19]. These achievements greatly stimulated the development of novel PI3K inhibitors, especially PI3K selective inhibitors.

Among the four isoforms, PI3K γ has been attracted more and more attention for its restricted expression in the hematopoietic systems, especially in leukocytes [20]. Thus, PI3K γ is considered as a valuable target to treat not only advanced solid tumors, leukemia and lymphoma, but also inflammatory and autoimmune diseases [21–23]. However, the high structural and sequential homology of these four PI3K isoforms is a huge hinder to acquire specific PI3K γ inhibitor [24]. Some selective PI3K γ inhibitors have been discovered with experimental methods and almost all of those were identified through screening against a broad panel of diverse kinases for each chemical scaffold [22,25,26]. It is known that these traditional experimental approaches are expensive and time-consuming [27]. Besides, it is reported that in the ATP-binding pocket of PI3K γ , the side chains of the residues distinguished from other isoforms are always rotated away from the

pocket [24]. The conventional methods are difficult to reveal these structural features at a molecular level. Therefore, computer-aided drug design (CADD) is an appropriate selection to aid in the discovery or design of PI3K γ inhibitors with a high degree of selectivity [28–30]. Thus, in this present study, a combined approach integrated bioactive evaluation and computer simulation was conducted to discover novel PI3K γ inhibitors. The whole workflow was given in Fig. 1. First, a machine learning-virtual screening (VS) model based on molecular docking with multi-PI3K γ conformations was built to screen the ChemDiv database, and some top-ranked inhibitors were purchased and submitted to bioassays. As a result, some potential PI3K γ selective inhibitors were identified. Particularly, JN-KI3 exhibits a high degree of PI3K γ -selective inhibition and specific anti-proliferative activity against hematologic malignancies. In the end, a systematic computational analysis utilizing molecular docking and molecular dynamic (MD) simulations was performed to study the selective-PI3K γ inhibition mechanism of JN-KI3.

Material and methods

Construction of VS model

Preparation of PI3K γ complexes

The workflow of the VS protocol is illustrated in Fig. 1. A total of 87 crystallographic structures of PI3K γ -inhibitor complexes were gathered and retrieved from the RCSB protein data bank (PDB, Table S1 in the supplementary information) [31]. All PI3K γ protein structures were prepared with Protein Preparation Wizard module of Schrödinger 9.0 to remove crystallographic waters, add hydrogen atoms, assign partial charges with the OPLS-2005 force fields [32], assign the protonated state. The missing side chains and loops were added using Prime module, and last, all protein structures were minimized until the root-mean-squared-deviation (RMSD) reached a maximum value of 0.3 Å, and other parameters were set as default. Then the residues within 10 Å of each co-crystallized ligand were reserved and structurally aligned with STAMP algorithm in VMD [33]. Afterward, the phylogenetic tree module in VMD was employed to calculate the phylogenetic tree based on the RMSD values and the result was illustrated in Fig. S1, all of them were divided into 10 categories and the complex with the highest resolution within each category were chosen and finally 10 representative complexes were selected to further docking simulation. Firstly, the “docking power” of these chosen complexes was evaluated with following steps: the co-crystallized ligands were redocked into the active binding pocket by Glide/SP (standard precision) and Glide/XP (extra precision)

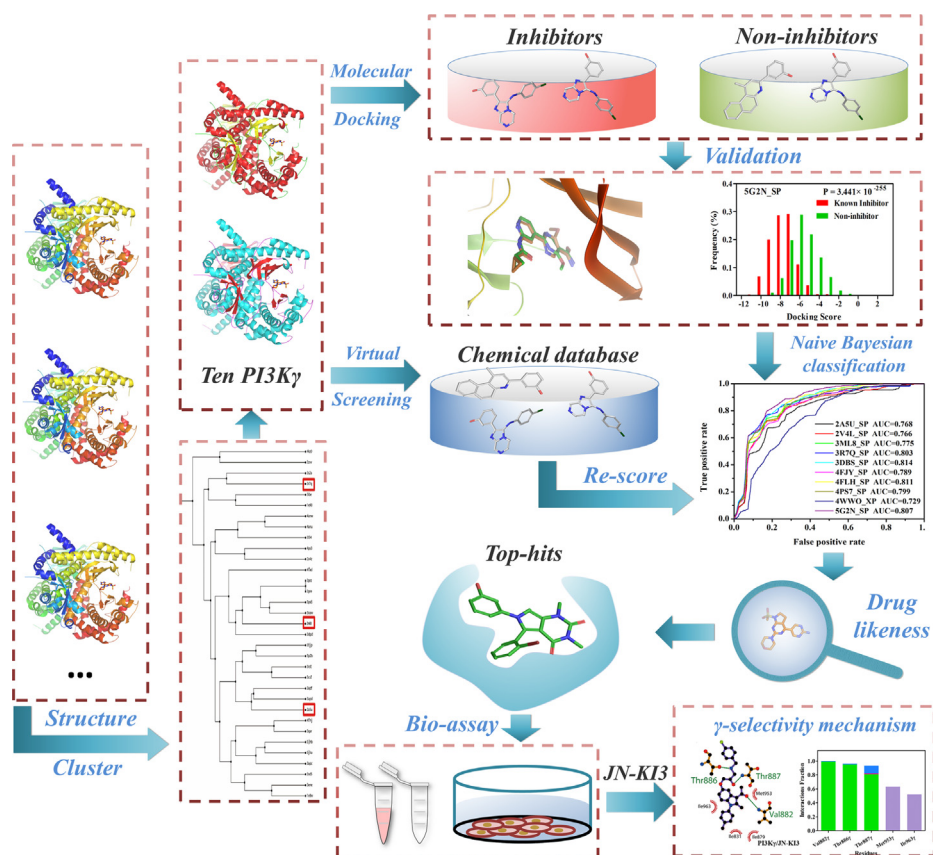


Fig. 1. The workflow of this study.

molecular docking methods, and then the RMSD between the docking results and the original conformations of inhibitors were calculated. Generally speaking, $\text{RMSD} \leq 2.0 \text{ \AA}$ represents the criterion of successful docking prediction [34].

Inhibitor/non-inhibitor validation set

In order to evaluate the “screening power” of the 10 complexes with the docking module, which represents the ability to distinguish the known PI3K γ inhibitors from non-inhibitors, 800 PI3K γ inhibitors, as an “inhibitor set”, with definite biological activity ($\text{IC}_{50} < 10 \text{ \mu M}$) were extracted from BindingDB database [35] using *Find Diverse Molecules* module of Discovery Studio 3.5 (DS3.5) software. Besides, 16,000 compounds were randomly selected from ChemDiv compound library with the *Find Diverse Molecules* in DS 3.5 to construct a “decoy set”, the ratio between inhibitors and decoys was 1:20. Both “inhibitor set” and “decoy set” were minimized under OPLS-2005 force field [2] using the *LigPrep* module of Schrödinger 9.0 with the default parameters set.

Validation of molecular docking

10 prepared PI3K γ complex were then submitted to perform molecular docking. the *Receptor Grid Generation* module of Schrödinger 9.0 was employed to generate a bounding box of size $10 \text{ \AA} \times 10 \text{ \AA} \times 10 \text{ \AA}$ within each PI3K γ structure, and the center of each box was defined through the co-crystallized ligand in the ATP binding site. And all prepared compounds in the validation set were then docked into the ATP binding site of these PI3K γ structures, and all docking poses were scored by the SP and XP scoring modes. The best binding pose of each compound was saved for the following analysis, and Student's *t*-test was used to measure the difference in the distribution of docking scores between inhibitor and non-inhibitors.

Integrated docking with multiple PI3K γ proteins

Consequently, a machine learning approach, naive Bayesian classification (NBC), based on these 10 PI3K γ structures was employed to evaluate the screening accuracy. The docking scores calculated by the *Glide* docking module were used as the independent variable (X), and 1/0 (1 for PI3K γ inhibitor and 0 for non-inhibitor) was used as the response variable (Y). Then, the predicting classifiers for VS model were generated following the *Create Bayesian Model* protocol in DS 3.5, and the ligand enrichment was determined through the area under ROC (receiver operating characteristic curve) value (AUC). The AUC represents the relationship between the true positive rate (active inhibitors) and the false positive rate (decoys), and a high AUC value indicates that the developed model contains a strong power to discriminate the positive inhibitors from the negative non-inhibitors [36].

Multi-conformational virtual screening in a sequential manner

Firstly, about 2,000,000 compounds from ChemDiv database were docking into the binding site of 10 PI3K γ structures with the preferred docking precision, respectively, and 10,000 top-ranked compounds were retained. And then, the best Bayesian classifier was then utilized to re-score these 10,000 compounds, and 2,000 compounds with top Bayesian scores were reserved. Afterward, these compounds were assessed the drug-likeness by *Filter by Lipinski and Veber Rules* module in DS3.5 [37] and the *rapid elimination of swill (REOS) rules* in Canvas [38], and 200 compounds were selected. Besides, to maintain structure diversity of screening compounds, the 200 compounds were structurally clustered through the *Find Similar Molecules by Fingerprints* module in DS3.5, the compounds with similarity coefficients higher than 0.8 were clustered into the same group. And then, 100 compounds with various scaffolds were chosen. The 2D-interactions patterns

between these 100 compounds and PI3K γ following illustrated by the *Ligand Interactions* module of Schrödinger. And the compounds interacting with the “hot residues” within the ATP binding pocket, which were identified by our previous work [39,40], were kept. Finally, the top 49 compounds with required interactions were selected as pro-hits for the following biological evaluations.

Promiscuity and ADMET assessment

The promiscuity of JN-KI3 was investigated by two online programs, Badapple [41] (bioactivity data associative promiscuity pattern learning engine, <http://pasilla.health.unm.edu/tomcat/badapple/badapple>) and Hit Dexter 2.0 [42] (<https://acm.zbh.uni-hamburg.de/hitdexter/>). For both tools, the SMILES (simplified molecular input line entry specification) format of JN-KI3 was entered into the input box and the results would be generated automatically. In addition, the ADMET (absorption, distribution, metabolism, excretion, and toxicity) properties were predicted using *QikProp* module of Schrödinger. This module was carried out in normal mode and predicted principal descriptors and physicochemical properties of JK-KI3.

Bio-assay evaluation

PI3K kinases activity in cell-free assays

The PI3K inhibitory activities of these pro-hits were all determined by ADP-Glo assay (Promega) [39]. For the initial screening, the compositions and optimized concentrations of the assay were listed as below: PI3K γ 0.625 $\mu\text{g/mL}$, PIP2:PS 50 $\mu\text{g/mL}$, compounds 10 μM , ATP 25 μM , IPI-145 and LY294002 [43] were used as positive controls. For the JN-KI3 kinases activity assays, the compositions and optimized concentrations were listed as follows: PI3K α 0.625 $\mu\text{g/mL}$, PI3K β 0.625 $\mu\text{g/mL}$, PI3K δ 0.625 $\mu\text{g/mL}$, PI3K γ 0.625 $\mu\text{g/mL}$, ATP 25 μM , PIP2:PS 50 $\mu\text{g/mL}$, PI-103 and LY294002 were used as positive controls. JN-KI3 and all positive compounds were serially diluted into required concentrations. In all cases, except for the control wells and background wells, the solution of PI3K enzymes was incubated with testing compounds in 384 plate for 45 min. 2.5 μL ATP/substrate mixture was added into the wells to initiate kinase reactions and incubated at room temperature for 1 h. Then, the reactions were stopped by addition of 5 μL ADP-Glo reagent and incubation for 120 min at room temperature. Before reading the luminescence signals of each well, 10 μL kinase detection buffer was added and incubated for 30 min at room temperature.

Cell lines and cell culture

The human cancer lines, MDA-MB-231, Patu8988, HepG2, A2780, LOVO, H1299, A549, HCT-8, SW480, 3AO, and MGC-803 were saved by the lab of Dr. Jian Jin, Jiangnan University. MCF-7 was purchased from the American Type Culture Collection (ATCC). Human malignant blood tumor cells, HL-60, U266, OPM2, OCI-My5, RPMI-8226, NCI-H929, Jurkat, LP-1, CCRF-CEM, K562, and U937, were provided by Dr. Xinliang Mao, Soochow University. MDA-MB-231, Patu8988, HepG2, A2780, LOVO, H1299, A549, HCT-8, SW480, 3AO, MGC-803, and MCF-7 were cultured in Dulbecco's Modified Eagle Medium (DMEM, Gibco); U266, RPMI-8226, OPM2, OCI-My5, NCI-H929 and LP-1 were cultured in Iscove's Modified Dulbecco's Medium (IMDM, Gibco). The rest of cell lines were cultured in RPMI-1640 medium (Gibco). All mediums were supplemented with 10% fetal bovine serum (FBS, Gibco), 100 $\mu\text{g/mL}$ penicillin and streptomycin, and all cells were maintained in a cell incubator with 5% CO₂ at 37°C.

Cell proliferation assay

All cells were incubated in 96-well culture plates with 100 μL medium in each well. The concentration of solid cells (MDA-MB-231, MCF-7, Patu8988, HepG2, A2780, 3AO, LOVO, HCT-8, SW480, A549, H1299, and MGC-803) was 3,000/well and the concentration of suspension cells (HL-60, U266, OPM2, OCI-My5, RPMI-8226, NCI-H929, Jurkat, LP-1, CCRF-CEM, K562, and U937) was 7,500/well. Cells were then treated with 5 μL compounds and positive inhibitors, IPI-145 and LY294002, diluted in the required concentration for 72 h. The viability of the cancer cells was evaluated by Thiazolyl Blue (MTT) assay. 10 μL of 5 mg/mL MTT was added to each well and the plate was incubated at 37°C for 4 h. Then, 100 μL MTT buffer was added to each well. After incubating the plate overnight, the absorbance of each well was measured at 550 nm by a microplate reader. All data were normalized to control groups (5 μL DMSO) and converted into the percent of living cells. All results were represented as the mean and standard deviation (SD) of the three independent measurements.

Western Blot assay

K562 and RPMI-8226 cells were cultured in 6-well plates with 1×10^6 cells per well and then treated with various concentrations of JN-KI3: 0, 2.5, 5, 10, and 20 μM . After 24 h, the cells of each well were collected and washed by PBS 3 times. The sedimentary cells were then incubated in an ice bath with 80 μL RIPA lysis buffer (Beyotime) for 20 min and then centrifuged at 12,000 rpm for 20 min. The supernatant was collected and its total concentration of protein was quantified using the BCA protein assay kit (Biosharp). Loading buffer (5 \times) was added to all protein samples prepared for Western Blot assays and boiled at 100°C for 5 min.

The inhibitory situation of PI3K/AKT (Protein kinase B) signaling pathway was then determined by Western Blot assays. The SDS-polyacrylamide gel electrophoresis (PAGE) was used to separate the proteins. All protein samples and Protein Marker (Proteintech) were loaded onto an acrylamide gel and ran for 30 min at 80 V within the stacking gel and for 1 h at 100 V with the separating gel. Then, the protein was electro-transferred onto an NC membrane at 100 V for 1 h. After that, the membrane was blocked in 5% skim milk diluted in TBST (1 \times) for 2 h and then the membrane was incubated with relevant primary antibody overnight at 4°C: Phospho-AKT (Thr308) (1: 1000, cat# 13038 T; Cell Signaling Technology), Phospho-AKT (Ser473) (1: 1000, cat# 4060 T; Cell Signaling Technology), AKT (pan) (1: 1000, cat# 4691 T; Cell Signaling Technology), caspase-3 (1: 1000, cat# sc-56053; Santa Cruz Biotechnology), PARP (1: 1000, cat# 9542S; Cell Signaling Technology), GAPDH (1: 5000, cat#60004-1-Ig; Santa Cruz Biotechnology). After 10-min washing in TBST (1 \times) for 3 times, the membrane was incubated with relevant secondary antibody at room temperature on a shaker for 1 h. And the membrane was washed for 4 times in TBST again before being imaged.

Flow cytometry assay

After being treated with JN-KI3 for 24 h, K562 and RPMI-8226 were stained with Annexin V-FITC/PI detection kit (Beyotime) and the apoptosis of the cells were detected using a flow cytometer (FACSCalibur, BD) following the instructions.

Theoretical studies on the PI3K γ selective inhibition mechanism of JN-KI3

Docking studies. The crystallographic structures with high resolutions of PI3K α (PDB ID: 6PYS) [44], PI3K β (PDB ID: 2Y3A) [45], PI3K δ (PDB ID: 6PYR) [44] and PI3K γ (PDB ID: 4ANV) [46] were stretched from the RCSB PDB. All structures were prepared in the *Protein Preparation Wizard* module of Schrödinger 9.0. The 3D-structures of Cpd5, Cpd36, Cpd38, and JN-KI3 were generated by

maestro and minimized in the *LigPrep* module. Then, a bounding box was generated on the ATP binding site of each complex with the center of crystallized ligand by using the *Receptor Grid Generation* module. Cpd5, Cpd36, and Cpd38 were docked into PI3K γ , while JN-KI3 was docked into the binding site of each complex, all docking programs were performed using *Glide SP* method.

MD simulations. Four PI3Ks/JN-KI3 complexes with the best conformations generated by molecular docking were used as initial structures to perform MD simulations by *Desmond* [47]. Each complex system was immersed in a solvent model with TIP3P water molecules and the boundary of the infiltration volume was extended to 10 Å in each direction. Then, each system was neutralized with Na⁺/Cl⁻ counter ions and minimized under the OPLS-2005 force field [2]. Afterward, four complexes were submitted to MD simulations following the default NPT and NVT ensemble protocols in *Desmond* program, a 200-ns MD simulation at the pressure of 1 atm maintained by Martyn-Tobias-Klein pressure bath [48] and at the temperature of 300 K maintained by Nose-Hoover Chain thermostat [49] was performed for each system. The Smooth Particle Mesh Ewald method [50] was used to analyze the electrostatic interaction forces between the complexes. And the RMSDs of the PI3Ks protein backbones and the RMSF (root-mean-squared-fluctuation) value of each atom in JN-KI3 were calculated.

MM/GBSA free energy calculation. The binding free energy (ΔG_{Bind}) for each system was calculated by using *Prime MM/GBSA* (Molecular Mechanics/Generalized Born Surface Area) module employing an equation:

$$\Delta G_{\text{Bind}} = G_{\text{complex}} - (G_{\text{protein}} + G_{\text{ligand}})$$

Where G_{complex} , G_{protein} and G_{ligand} are the prime energies of the optimized complex, free receptor and free ligand, respectively [51].

Results and discussion

Performance of the VS model

Accumulative studies have shown that multi-conformational virtual screening, which could mimic the induced-fit effect of the protein, in a sequential or parallel manner could be the most appropriate to balance efficiency and precision of VS than the conventional VS, which usually uses single one protein with “rigid” structure to guarantee the optimum efficiency of VS. Therefore, 87 PI3K γ crystallographic structures from PDB were collected and then divided into 10 conformational types after the clustering analysis. The complex with the highest resolution in each class was chosen and finally 10 representative complexes were selected, namely, 2A5U (Resolution: 2.70 Å) [22], 2V4L (2.50 Å) [52], 3DBS (2.80 Å) [53], 3ML8 (2.70 Å) [54], 3R7Q (2.50 Å) [55], 4FJY (2.90 Å) [56], 4FLH (2.60 Å) [57], 4PS7 (2.69 Å) [58], 4WWO (2.30 Å) [59] and 5G2N (2.68 Å) [60] (PDB ID). In order to estimate the precision and stability of these docking model systems, the “docking power” and “screening power” were evaluated, respectively. The “docking power”, which is a vital criterion of the reliability of molecular docking, presents the accuracy of poses prediction. For each PI3K γ complex, the crystallized ligand was re-docked into the binding site and the RMSD between the docking pose and its original conformation was calculated. The results were tabulated in Table 1, the RMSD of ten PI3K γ complexes were all <2.0 Å, which means that all of them contain remarkable predicting power through both *Glide/SP* or *Glide/XP* molecular docking methods.

On the other hand, the “screening power” was investigated, which exhibits an ability of the docking methods to distinguish the active PI3K γ inhibitors from non-inhibitors. Herein, 800 PI3K γ inhibitors with definite bio-activity and 16,000 non-inhibitors

were chosen to make up a validation set. All compounds in the dataset were all docked into ten PI3K γ proteins with SP and XP modes, respectively. The distributions of two docking scores of each protein were illustrated, and the T-test was carried out to evaluate the discrimination capacity of each protein with P-value. As shown in Table 1, both SP and XP could accurately distinguish the inhibitors from non-inhibitors for ten PI3K γ proteins (P-value < 0.05), but overall, the performance of SP shows better than XP in each system, except 4WWO (Fig. 2). Take 2A5U as an example, the P-value of SP mode is 1.612×10^{-158} , which is much < 9.675×10^{-128} , the P-value of XP. Some studies have demonstrated that even though XP is the extra precision mode of the *Glide* module and considered to be more accurate, the performance of SP is not always worse than it. Therefore, in our studied PI3K γ systems, except 4WWO, SP mode with superior “screening power” would be adopted.

Next, the data matrix consisting of the docking scores from the above validation protocols was utilized to build the NBC model. The capability to distinguish between inhibitors and non-inhibitors for the NBC model was measured through the AUC value. Firstly, ten NBC models were constructed based on a single docking score for each complex, as summarized in Fig. 2K. The NBC model of 3DBS_SP (both inhibitors and non-inhibitors were docked into protein following *Glide/SP* protocol) shows the best predicting power and the AUC value is 0.814. The AUC value of each system is 0.768 (2A5U_SP), 0.766 (2V4L_SP), 0.775 (3ML8_SP), 0.803 (3R7Q_SP), 0.789 (4FJY_SP), 0.811 (4FLH_SP), 0.799 (4PS7_SP), 0.729 (4WWO_XP) and 0.807 (5G2N_SP), respectively (Fig. 2K). Generally, the AUC value > 0.7 indicates that the model contains a satisfactory prediction power, thus a novel NBC model based on the combined docking scores of the ten PI3K γ proteins was built up, as shown in Fig. 2L, the AUC value of this model is as high as 0.906, showing an excellent prediction for PI3K γ inhibitors.

JN-KI3 selectively inhibit PI3K γ

The 49 pro-hits identified from VS were numbered as Cpd1 to Cpd49. The cell-free PI3K γ inhibitory activities of these hits were firstly validated by ADP-Glo assay. The reported inhibitors, IPI-145 and LY294002, were tested as positive controls. The PI3K γ -inhibitory activity of each hit was primitively validated at the concentration of 10 μ M and the results were shown in Fig. 3A. At first glance, the marketed drug, IPI-145, showed the strongest inhibitory activity but it is encouraging that there are four hits with the inhibitory percent exceeding 50%, namely, Cpd5, JN-KI3 (Cpd14), Cpd36 and Cpd38. Among these four compounds, JN-KI3 has the most satisfying activity with almost 60% inhibitory percent to PI3K γ , the 2D structure of JN-KI3 is illustrated in Table 2. The molecular docking results between these four compounds and PI3K γ show that these compounds all form hydrogen bonds (H-bond) with Val882 of PI3K γ (Fig. S2), Val882 have been identified as a core residue, which could form characteristic H-bond in almost all of the PI3K γ /inhibitors complexes. Therefore, these four compounds all cause varying degrees of PI3K γ inhibition. The alignment of the four compounds in the binding pocket shows JN-KI3 could form stronger hydrophobic interaction with PI3K γ because of its chlorine phenyl group (Fig. S2A). The modeling results also reveal that JN-KI3 contains a novel scaffold different from the classical propeller-shaped core structure, like IPI-549. Then, the selective inhibition of JN-KI3 on other PI3K isoforms was evaluated and the potent pan-PI3K inhibitor, PI-103, was used as the positive control, the results summarized in Table 2. The IC₅₀ value of JN-KI3 against PI3K γ is 3,873 nM, whose inhibitory potency is near to LY294002. Though JN-KI3 shows lower bio-activity on PI3Ks than PI-103, encouragingly, it exhibits a significant specificity to PI3K γ , as shown in Table 2, the IC₅₀ values of

Table 1
The docking power, screening power, and crucial interactions of ten PI3K γ crystal structures.

PDB ID	RMSD (Å)		P value		Interactions
	SP	XP	SP	XP	
2A5U	0.776	0.746	1.612×10^{-158}	9.675×10^{-128}	Asp964, Asp836
2V4L	0.789	0.779	2.740×10^{-193}	3.007×10^{-163}	Val882, Lys833
3DBS	0.830	0.816	1.961×10^{-227}	3.239×10^{-208}	Val882, Tyr867
3ML8	0.810	0.801	4.483×10^{-199}	4.384×10^{-195}	Val882, Asp964
3R7Q	0.818	0.803	1.868×10^{-205}	7.619×10^{-191}	Val882, Tyr867
4FJY	0.793	0.753	8.318×10^{-183}	5.004×10^{-125}	Val882
4FLH	0.824	0.799	2.158×10^{-212}	2.889×10^{-164}	Val882, Lys833
4PS7	0.816	0.798	1.970×10^{-198}	3.452×10^{-178}	Val882, Tyr867
4WWO	0.721	0.171	4.909×10^{-84}	7.920×10^{-103}	Val882
5G2N	0.849	0.835	3.441×10^{-255}	6.537×10^{-253}	Val88, Lys833

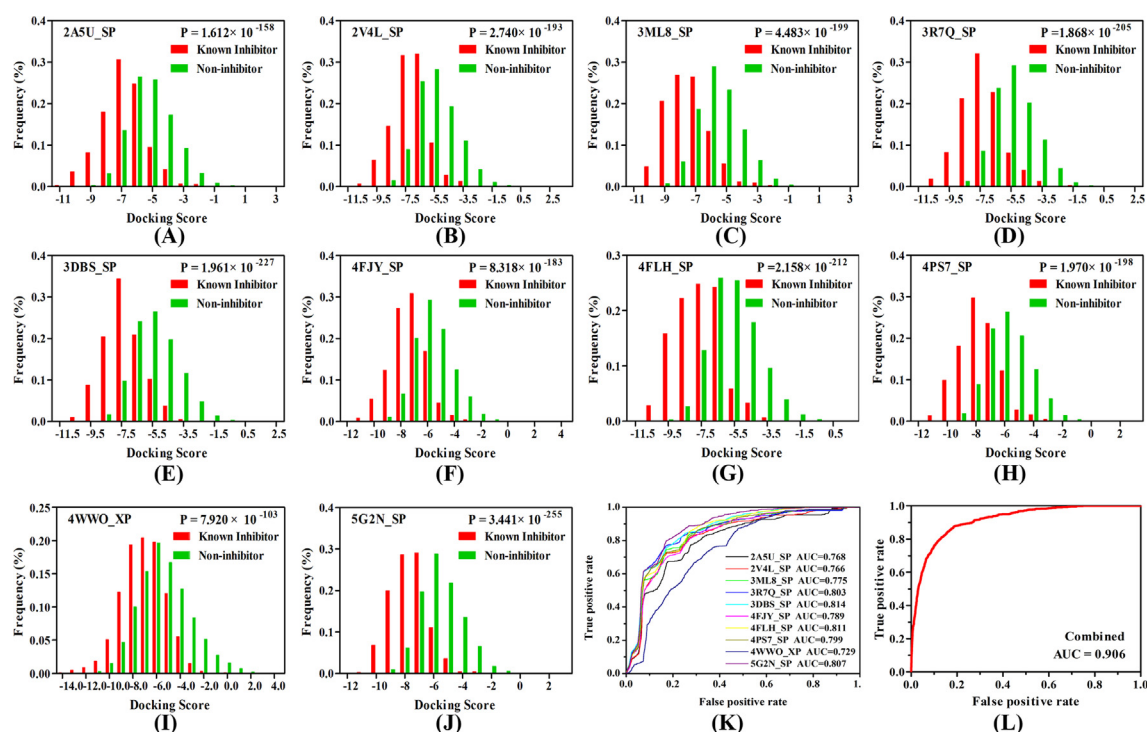


Fig. 2. (A–J) Distributions of the docking scores of the inhibitor (red)/noninhibitor (green) for each PI3K γ protein with the best discrimination power; (K) the ROC curve of the naive Bayesian classifier based on every single docking score; (L) the ROC curve of the naive Bayesian classifier based on the combined docking scores.

JN-KI3 against other three isoforms are all >20,000 nM. Comparing to JN-PK1, which is an effective hit identified from our previous traditional VS work, JN-KI3 appeared not only a more significant PI3K γ inhibitory activity, but also a higher selectivity against PI3K γ . This result strongly proves that the VS integrated a machine learning based on multi-conformational PI3K γ could effectively discover novel selective PI3K γ inhibitors.

The promiscuity and ADMET assessments for JN-KI3

Pan-assay interference compounds (PAINS) analysis was used to investigate how far JN-KI3 could be flagged as a PAINS compound. PAINS refer to a series of promiscuous compounds specifically binding to different macromolecular targets and leading to misleading false-positive results in experimental assays. Therein, two available promiscuous predicting algorithms, Hit Dexter 2.0 and Badapple, were utilized to examine whether JN-KI3 could be categorized as PAINS. The detailed promiscuity analysis result of JN-KI3 using Hit Dexter 2.0 is available on the website (<https://nerdd.zhb.uni-hamburg.de/hitdexter/result/c1ac770f-753e-455b-8c66->

[a5ed2337dbfd](#)). JN-KI3 is predicted as non-promiscuous by the PSA (primary screening assays) classifier with a probability of 0.90 and the CDRA (confirmatory dose–response assays) classifier with a probability of 1.00 at moderate confidence. Besides, JN-KI3 shows the low promiscuous probability values even at high confidence, 0.26 for PSA, and 0.17 for CDRA (Fig. S3). It demonstrates that JN-KI3 would be a specific compound rather than a promiscuous one. Promiscuity screening data of Badapple are listed in Table 3. Scaf1, the indolyl group of JN-KI3, is found to have a pScore value higher than 300, accompanied with a “True” result inDrug database. The other scaffold, Scaf2, 1-phenyl-indole, presented a moderate pScore value with a “True” result inDrug database. These results suggest both promiscuity and drug-likeness probability of JN-KI3. However, no pScore was generated for Scaf3 and Scaf4, and the inDrug values are both “False”, indicating the absence of the scaffolds in the drug database.

Besides, *in silico* ADMET of JN-KI3 were calculated to predict the pharmacological properties. Table 3 shows that almost all properties are within the acceptable range. For instance, all the logP values are within the optimal range, the human oral absorption

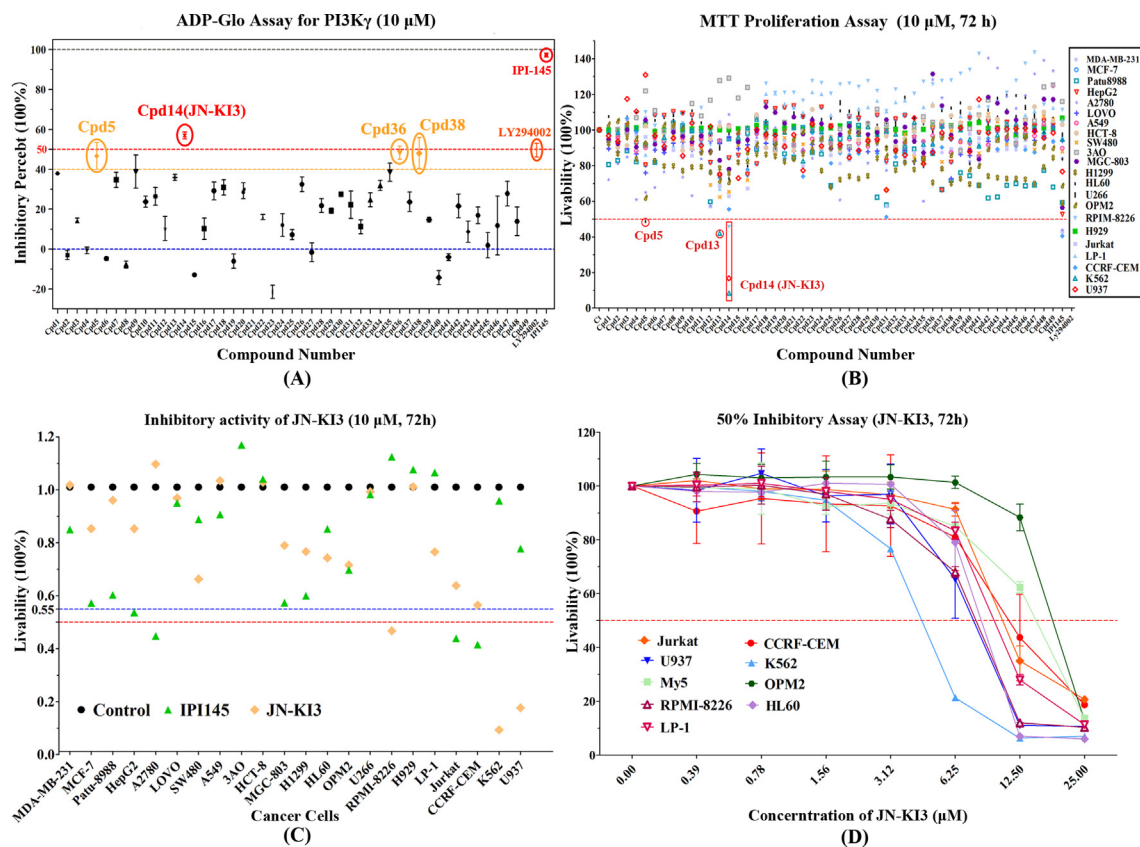
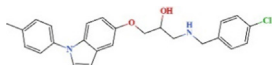
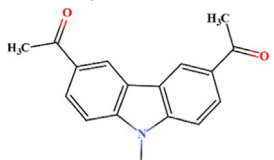
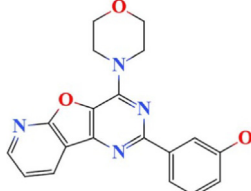
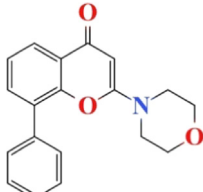


Fig. 3. (A) The cell-free PI3K γ inhibitory activities of 49 hits and two positive inhibitors, IPI-145 and LY294002; (B) the anti-proliferation effects towards multiple tumor cells of 49 hits and two positive inhibitors, IPI-145 and LY294002; (C) the anti-proliferation effects towards multiple tumor cells of JN-KI3 and IPI-145; (D) the anti-proliferation effects towards multiple malignant tumor cells of JN-KI3 with the gradient of concentrations.

Table 2

The 2D-structures and the cell-free inhibitory activity values (IC₅₀) of JN-KI3 and the positive reference compounds JN-PK1, PI-103, and LY294002.

Compounds	Structures	Cell-free inhibitory IC ₅₀ (nM) ^a			
		PI3K γ	PI3K α	PI3K β	PI3K δ
JN-KI3		3,873	>20,000	>20,000	>20,000
JN-PK1		7,490	11,300	>20,000	>20,000
PI-103		50	3.8	10	5.1
LY294002		2,980	1,660	2,580	780

^a Average of triple tests.

(PHOA) of JN-KI3 is close to the highest recommended values, 100%. All these predictions indicate that JN-KI3 exhibits optimum drug-like properties.

JN-KI3 selectively anti-proliferate against hematologic cancer cells

At the same time, the anti-proliferative activity of each hit towards different human cancer cells was evaluated, including breast cancer cells (MDA-MB-231, MCF-7), pancreatic cancer cell (Patu8988), liver cancer cell (HepG2), ovarian cancer cells (A2780, 3AO), colon cancer cells (LOVO, HCT-8, SW480), lung cancer cells (A549, H1299), gastric cancer cell (MGC-803), and hematologic malignancies cells (HL-60, U266, OPM2, RPMI-8226, NCI-H929, Jurkat, LP-1, CCRF-CEM, K562, U937). IPI-145 and LY294002 were still used as positive controls. The anti-proliferative activity of each hit was shown as the livability of the cells. Fig. 3B shows that there are three hits considerably inhibiting the proliferation of some cancer cell lines. To be specific, Cpd5 could suppress the proliferation of acute promyelocytic leukemia (HL-60), Cpd13 could inhibit chronic myelogenous leukemia (K562). It is a pity that the results from the cellular experiments are not in good agreement with those of above cell-free assays, such as Cpd36 and Cpd38, which show little anti-tumor effect. But luckily, JN-KI3 show potently suppressed proliferation in some cell lines and more interestingly, JN-KI3 seems to prefer to inhibit the proliferation of hematologic cancer cell lines, such as K562 and multiple myeloma cell lines (RPMI-8226 and U937), and the inhibition effect is even stronger than IPI-145 (Fig. 3C). As discussed above, PI3K γ is mainly distributed and expressed in the hematopoietic systems, that may lead to the specific inhibition against hematologic cancer cell lines. To test this hypothesis, more hematologic tumor cell lines were treated with JN-KI3, including four human leukemia cells (HL-60, Jurkat, CCRF-CEM, K562), four multiple myeloma cells (OPM2, OCI-My5, LP-1, RPMI-8226) and one lymphoma cells (U937). As shown in Fig. 3D, the proliferation of all cells was decreased in a concentration-dependent manner, especially K562, which show significant sensitivity to JN-KI3 at a low concentration.

JN-KI3 induce apoptosis of hematologic cancer cells with selective inhibition on PI3K/AKT signaling pathway

As it has been widely reported that PI3K γ /AKT signaling pathway play central roles in regulating the survival and proliferative activities in hematologic malignancies. To investigate the inhibition of JN-KI3 to PI3K at the cellular level, immunoblotting assays were performed with the two sensitive cell lines, K562, and RPMI-8226 (8226). AKT is a node protein downstream of the PI3K signaling pathway. The inhibition of PI3K γ kinase activity can suppress the phosphorylation of AKT at Thr308 and Ser473 sites. Thus, the inhibitory activity against PI3K of JN-KI3 at a cellular level was verified using AKT phosphorylation as a readout. As shown in Fig. 4A & B, after treating with the increasing concentration of JN-KI3 for 24 h, AKT phosphorylation at Thr308 and Ser473 sites in K562 and 8226 cell lines were both markedly decreased, and the inhibition was caused even at a concentration as low as 2.5 μ M, while the expression of total AKT (t-AKT) was not affected. In addition, both K562 and 8226 cell lines were treated with 20 μ M JN-KI3 for the indicated time periods. As shown in Fig. 4C & D, the phosphorylation level of AKT at both sites was significantly inhibited with the prolongation of the time of JN-KI3 action. Similarly, t-AKT was not markedly affected. All the above results indicated that JN-KI3 would effectively inhibit PI3K/AKT signaling with a concentration- and time-dependent manners in hematologic cancer cells.

Those above results suggested that JN-KI3 could specifically inhibit PI3K γ both at the cell-free and the cellular level, and it selectively suppressed hematologic cancer cells. To further demonstrate whether JN-KI3 could induce the apoptosis of hematologic cells with the inhibition of PI3K γ , K562 and 8226 were treated with JN-KI3 with increased duration or concentrations, and the relative levels of two apoptosis biomarkers, PARP (poly ADP-ribose polymerase) and caspase-3 were detected and the results were illustrated in Fig. 4. Caspase-3 belongs to the caspase family of cysteine proteases, which are the key mediators of cell apoptosis. Caspase-3 cleaves the death substrate PARP to a specific 89 kDa form observed during apoptosis. Fig. 4A & B show that after incubating with the increasing concentrations of JN-KI3, the cleavage levels of PARP and caspase-3 in K562 and 8226 cell lines were obviously increased and showing in the dependent manner of concentration. Then, a time-course study was conducted, and both K562 and 8226 treated with 20 μ M JN-KI3 activated the PARP and caspase-3 following increased incubation time (Fig. 4C & D). The results demonstrated that the cleavage level of Caspase-3 and PARP in both cell lines significantly increased after a short time (6 h) of incubation with JN-KI3.

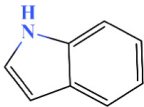
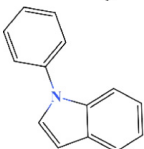
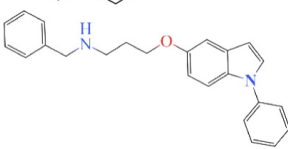
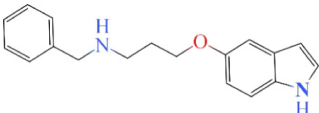
To further observe the induction of apoptosis by JN-KI3, Annexin V-FITC/PI double staining was performed to K562 and 8226 treated with increasing concentrations of JN-KI3 for 24 h, and then flow cytometry was utilized to observe the apoptotic cancer cells. As shown in Fig. 4E, JN-KI3 could induce the apoptosis of K562 at considerably low concentration, there was 41.2%, 47.5% and 65.7% of K562 cells occurring apoptosis after treating with 2.5, 5 and 10 μ M JN-KI3 for 24 h, respectively. Comparing to K562, 8226 presented moderate cellular apoptosis, about 20.43% of 8226 cells occurred definite apoptosis at a JN-KI3 concentration up to 10 μ M (Fig. 4F). These results are good agreement with those in cell proliferation bioassay. To sum up, JN-KI3 could induce apoptosis of hematologic cancer cells in association with its potent PI3K γ inhibition.

Theoretical studies on the PI3K γ selective inhibition mechanism of JN-KI3

In order to reveal the mechanism of selective inhibition of PI3K γ by JN-KI3 at a molecular level, a computational strategy integrating molecular docking, MD simulation and free energy calculations was employed. JN-KI3 was firstly docked into the ATP-binding pocket of four PI3K isoforms and the docking scores were listed in Table 4. It is delighted to find that the docking scores are consistent with the experimental inhibitory activities. The docking score of PI3K γ /JN-KI3 is -7.841 kcal/mol, which is higher than those of PI3K α /JN-KI3 (-6.730 kcal/mol), PI3K β /JN-KI3 (-6.640 kcal/mol) and PI3K δ /JN-KI3 (-6.018 kcal/mol). It roughly demonstrated that JN-KI3 has a stronger binding affinity to PI3K γ than the other three PI3K isoforms.

To further estimate the dynamic behavior of PI3Ks after binding to JN-KI3, the MD simulations were implemented and the docking poses from molecular docking studies (Fig. S4) were served as initial structures. The backbone RMSD values of four complexes were illustrated in Fig. S5, which indicated each system reached equilibrium in a short time after the simulations began. When the systems were stable, MM/GBSA method was utilized to calculate the binding free energy of each system. All results are listed in Table 4. The binding free energies of PI3K α /JN-KI3, PI3K β /JN-KI3, PI3K δ /JN-KI3, and PI3K γ /JN-KI3 are -42.832 , -36.875 , -49.441 and -64.981 kcal/mol, respectively. The predicted binding free energy of PI3K γ /JN-KI3 is greatly lower than the other three systems, which suggest that JN-KI3 binds to PI3K γ most tightly and it agrees with the above experimental and docking results.

Table 3
The pScore and inDrug values from Badapple data base, and the predicted ADMET properties of JN-KI3.

Compound	Scaffold Number	Scaffold Structure	pScore ^a	inDrug ^b
JN-KI3	Scaf1		370	True
	Scaf2		186	True
	Scaf3		None	False
	Scaf4		None	False

ADMET Prediction

Properties ^c	Value	Optimal range	Properties	Value	Optimal range
CNS	1	-2 - +2	polrz	51.04	13.0–70.0
logPC16	16.27	4.0–18.0	logPoct	23.54	8.0–35.0
logPw	11.51	4.0–45.0	logPo/w	5.53	-2.0–6.5
logS	-6.31	-6.5–0.5	ClogS	-6.67	-6.5–0.5
logHERG	-7.53	concern below -5	PCaco	364.52	<25 poor,>500 great
logBB	-0.37	-3.0–1.2	PMDCK	453.07	<25 poor,>500 great
logKp	-3.08	-8.0 - -1.0	logKhsa	1.05	-1.5–1.5
PHOA	92.20	>80% is high<25% is poor	rtvFG	0	0–2

^a pScore values advisory: <100 (low), means no indication; 100–300 (moderate), means weak indication of promiscuity; >300 (high), means strong indication of promiscuity.

^b inDrug results: true, means it was found in the drug data base; false, means not found.

^c properties: CNS, predicted central nervous system activity on a -2 (inactive) to +2 (active) scale; Polrz, predicted polarizability in cubic angstroms; logPC16, predicted hexadecane/gas partition coefficient; logPoct, predicted octanol/gas partition coefficient; logPw, predicted water/gas partition coefficient; logPo/w, predicted octanol/water partition coefficient; logS, predicted aqueous solubility; ClogS, conformation-independent predicted aqueous solubility; logHERG, predicted IC₅₀ value for blockage of HERG K⁺ channels; PCaco, predicted apparent Caco-2 cell permeability in nm/sec; logBB, predicted brain/blood partition coefficient; PMDCK, predicted apparent MDCK cell permeability in nm/sec. logKp, predicted skin permeability; logKhsa, prediction of binding to human serum albumin; PHOA, predicted human oral absorption on 0 to 100% scale; rtvFG, Number of reactive functional groups.

To further uncover the interaction modes between JN-KI3 and PI3Ks in a dynamic process, the dominant interactions, including H-bond, hydrophobic, ionic interactions (Ionic) and hydrogen bonds through water molecular bridge (Water Bridge), between key residues of each PI3K isoform and JN-KI3 were elucidated. As shown in Fig. 5, the carbonyl group of JN-KI3 formed an H-bond with Val residue in all four PI3K isoforms, namely, Val851 α , Val848 β , Val828 δ , and Val882 γ . After a sequence comparison and structural alignment, it suggested that these Val residues were conserved and located at the similar position at the hinge region within the ATP-binding pocket in all four isoforms. The hinge region is one of the four well-depicted regions in the ATP-binding pocket playing a significant role in determining the binding affinities between PI3Ks and small molecular inhibitors. As for PI3K α /JN-KI3, there were hydrophobic interactions between Trp780/Ile800/Ile932 and JN-KI3 (Fig. 5A). As for PI3K β /JN-KI3, Glu852 and Asp856 formed Water Bridge interactions with the free hydroxyl group and the secondary amino group of JN-KI3, respectively. Moreover, Ile930 formed a hydrophobic interaction with JN-KI3 (Fig. 5B). As for PI3K δ /JN-KI3, Trp760 formed a Pi-Pi interaction with the indole ring of JN-KI3, which almost dominated the nonpolar contribution in PI3K δ . In addition, there was a Water Bridge between Asp832 and JN-KI3 (Fig. 5C). As for PI3K γ /JN-KI3, except for Val882, Thr887 formed an H-bond with the free hydroxyl group of JN-KI3, and Thr886 formed another H-bond with the

free amino group of JN-KI3. As far as we know, these characteristic H-bonds are less common compared to most of the reported PI3K inhibitors. Besides, there were two strong hydrophobic interactions between Met953/Ile963 and JN-KI3 (Fig. 5D). Thus, the extra H-bonds and the stronger hydrophobic interactions between JN-KI3 and PI3K γ were deemed as the critical reason for the PI3K γ selective inhibition of JN-KI3.

Finally, the RMSF value of each atom of JN-KI3 was calculated, the atoms forming potent interactions with PI3Ks would be impeded to fluctuate and thus show extremely low values. As a whole, JN-KI3 exhibited less fluctuate in PI3K γ system (Fig. 6B), and it indicated JN-KI3 preferred to bind to PI3K γ . Specifically, the carbonyl group (atom index: 11 and 12), the indole ring (atom index: 1–9), P-methylphenyl at 9 position (atom index: 14–20) were all bind to PI3Ks with almost same interacted effect (green colored in Fig. 6A). Comparing the binding poses before and after the MD simulation, these groups show little fluctuation in the PI3K γ binding region (Fig. S6). The H-bond was always maintained between Val882 and the carbonyl group, while Met953 and Ile963 still form strong hydrophobic interactions with JN-KI3 (Fig. 6C & D). Therefore, this motif of JN-KI3 is vital for the satisfactory binding affinity to PI3K γ . However, the motif colored in red of JN-KI3 presented weak interactions with class IA PI3K isoforms, especially the chlorine phenyl (atom index: 26–32 and 34). Interestingly, the RMSF values of these atoms in PI3K γ /JN-KI3 were far lower than

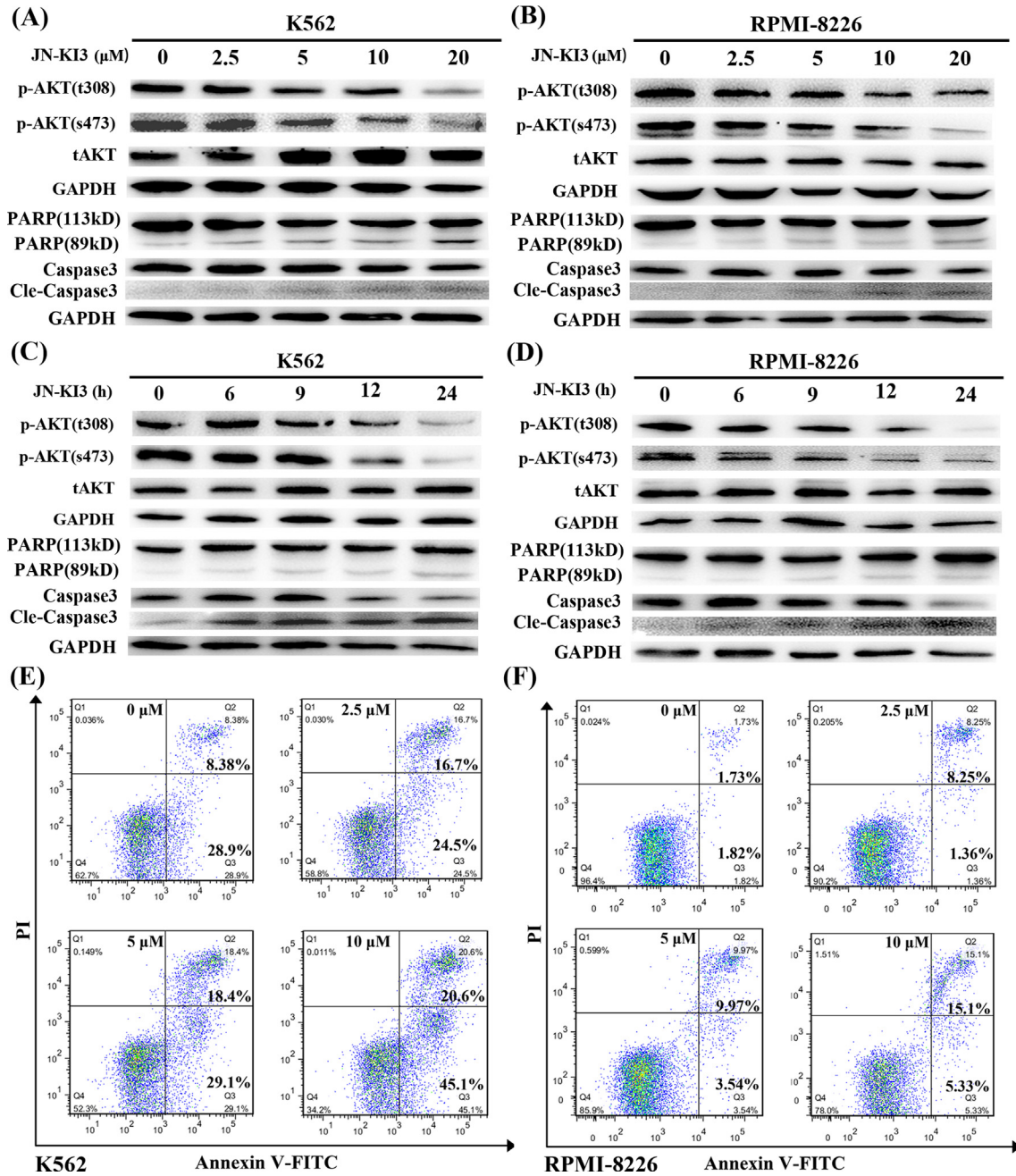


Fig. 4. JN-KI3 inhibited PI3K/AKT signaling pathway and induced apoptosis of (A) K562 and (B) RPMI-8226 cell lines at different concentrations from 0 to 20 μM after 24 h incubation. JN-KI3 inhibited PI3K/AKT signaling pathway and induced apoptosis of (C) K562 and (D) RPMI-8226 cell lines at different times from 0 to 24 h for 20 μM concentration. JN-KI3 induced apoptosis of hematologic malignancies illustrating by flow cytometry. Apoptosis of (E) K562 and (F) RPMI-8226 cell lines treated with different concentrations of JN-KI3 (from 0 μM to 10 μM) for 24 h.

Table 4

The docking scores and predicted binding free energies of JN-KI3/PI3Ks, and the inhibitory activities against PI3Ks of JN-KI3.

JN-KI3	PI3K γ	PI3K α	PI3K β	PI3K δ
Docking Scores (kcal/mol)	-7.841	-6.730	-6.640	-6.018
Binding free energy (kcal/mol)	-64.981	-42.832	-36.875	-49.441
IC ₅₀ (μM)	3.873	> 20	> 20	> 20

the values in other systems. On the other hand, the H-bond between JN-KI3 and Ala885 lost after MD simulation (Fig. 6C), the motif including chlorine phenyl (atom index: 21–34) had

significant ligand torsions (Fig. S6C), that made the motif prefer to bias Thr886 and Thr887, and lastly formed two strong H-bonds with these two residues (Fig. 6D). Thus, all these results

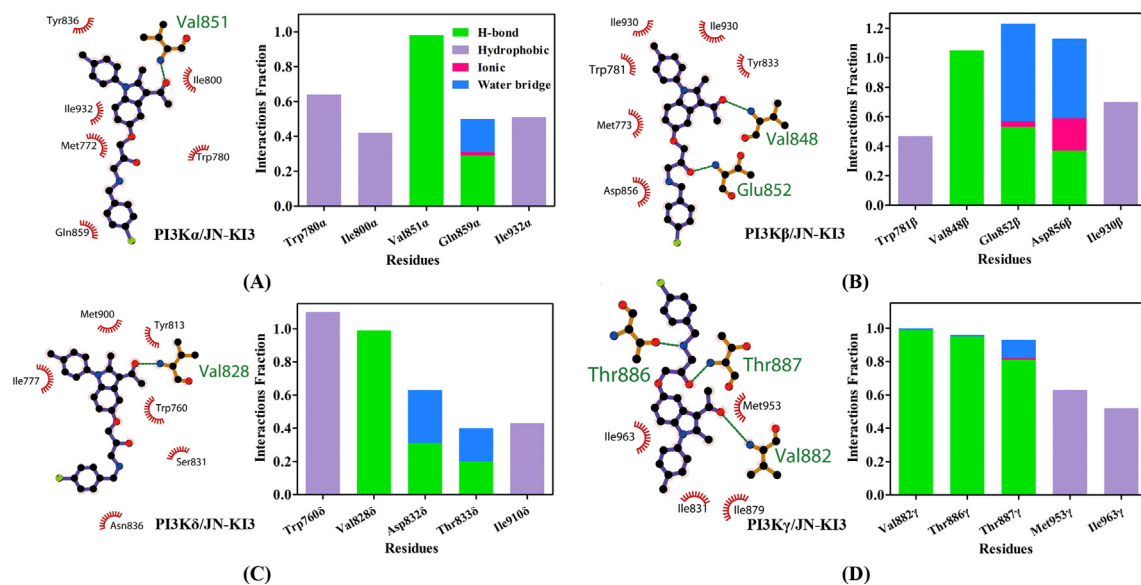


Fig. 5. 2D interaction patterns and protein–ligand occupancy histogram of (A) PI3K α /JN-KI3; (B) PI3K β /JN-KI3; (C) PI3K δ /JN-KI3; (D) PI3K γ /JN-KI3 complexes.

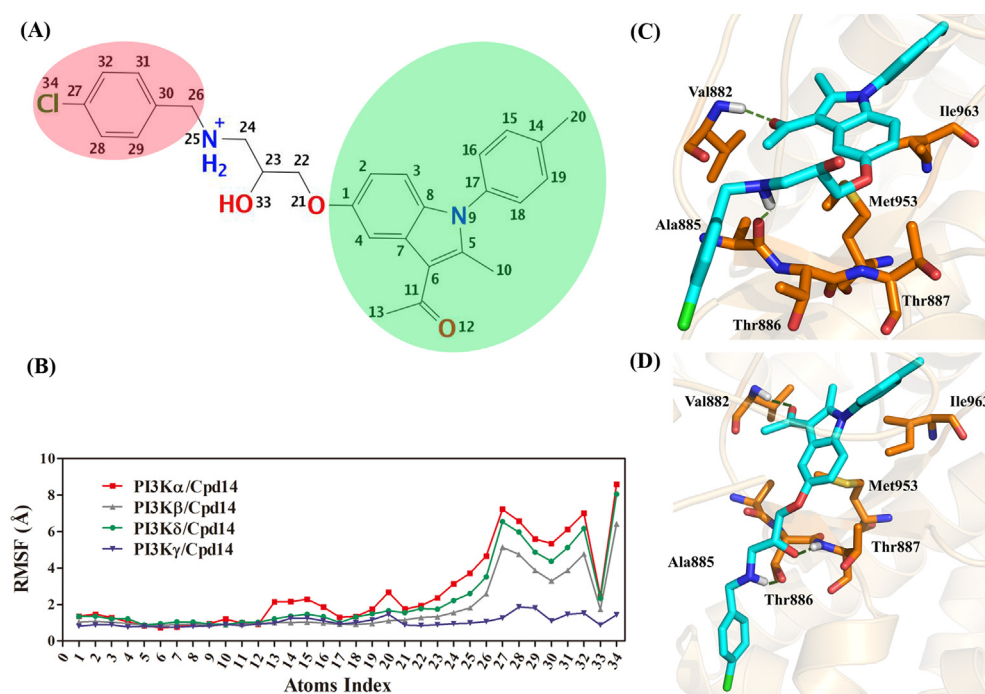


Fig. 6. (A) the 2D-structure labeled with atomic numbers; (B) the ligand RMSF value of JN-KI3; (C) the 3D-interaction diagrams between JN-KI3 and PI3K γ before MD simulation (H-bond colored in green); (D) the 3D-interaction diagrams between JN-KI3 and PI3K γ after MD simulation (H-bond colored in green).

are supposed to be responsible for the PI3K γ selective inhibition of JN-KI3.

Conclusion

In the present study, a machine learning-based VS with multiple protein structures was developed to screen against a large chemical library. This integrated VS model exhibits more precision prediction through mimicking the induced-fit effect of drug target than conventional VS, and the sequential manner during this protocol could be more appropriate to balance the efficiency and precision of VS. The developed NBC model integrating ten PI3K γ

proteins showed a satisfactory prediction power against PI3K γ inhibitors with the AUC value as high as 0.906, indicating that the VS with multiple PI3K γ structures would get much better performance and higher enrichment rate than that based on any single PI3K γ structure. After the evaluation of drug-likeness with the Lipinski and Veber rules and REOS, 49 VS-hits interacting with the “hot residues” within the ATP binding pocket of PI3K γ were screened out, and then, all compounds were submitted to a series of bio-assay studies. Firstly, the PI3K γ inhibitory activities of these hits were preliminarily validated by the cell-free assay, and four (4 in 49) compounds show over 50% inhibitory percent at a concentration of 10 μ M. Among them, JN-KI3 exhibits the most potent

selective PI3K γ inhibitory bioactivity, the IC₅₀ against PI3K γ is 3,873 nM. And, even more crucially, JN-KI3 shows a significant specificity to PI3K γ , while there is no inhibitory effect on Class IA PI3Ks even at concentrations higher than 20,000 nM. It suggests that the novel integrated VS strongly manifests the robustness to find new PI3K γ inhibitors. Meanwhile, the *in silico* PAINS and ADMET assessments indicated that JN-KI3 contains appropriate drug-like properties. Subsequently, dozens of common human cancer cell lines were treated with JN-KI3, respectively, and it is interesting that JN-KI3 prefers to inhibit the proliferation of hematologic cancer cell lines, the inhibition effect on some hematologic cancer cells is even stronger than IPI-145, which is consistent with the main distribution and expression of PI3K γ in the hematopoietic systems. Therefore, PI3K γ would be a suitable therapeutic target for hematologic cancers. Immunoblotting analysis revealed that JN-KI3 would effectively inhibit PI3K/AKT signaling with concentration- and time-dependent manners in hematologic cancer cells even at a low concentration. The further studies at the cellular models show that JN-KI3 could significantly induce apoptosis of hematologic cancer cells. The potent selective inhibition on PI3K γ of JN-KI3 resulted in the significant cleavage of two apoptosis biomarkers, PARP and caspase-3, and finally led to distinct apoptosis of the cell lines with dose- and time-dependent manners. Lastly, the selective inhibition mechanism of JN-KI3 against PI3K γ was uncovered by a theoretical study combining molecular docking, MD simulation, and free energy calculations. The results reveal that JN-KI3 contains the highest binding free energy against PI3K γ than Class IA isoforms, which is in good agreement with the experimental bioactivities. In addition, some key residues influencing γ isoform-selective inhibition of JN-KI3 were highlighted, such as Val882, Thr886, Thr887, Met953, and Ile963, these key interactions are less common compared to most of the reported PI3K γ inhibitors, indicating that JN-KI3 has novel structural characteristics as a selective PI3K γ inhibitor. On the other hand, some structural features of JN-KI3 critical to the γ -isoform preferred binding affinity were outstood, the chlorine phenyl of JN-KI3 formed stronger interactions with PI3K γ than Class IA isoforms, which makes a favorable contribution for specific inhibition on PI3K γ . All results could provide some significant guidance for the further rational design of JN-KI3.

Author Contributions

ZJ, LH, HG, JJ developed the study concept and design. LK performed the modeling studies and the bio-assay evaluation. ZJ, LK, ZX carried out the data analysis. XL provided software. ZJ, LK, CY drafted the manuscript, CY, LH, HG, JJ approved the manuscript.

Declaration of Competing Interest

The authors declare that they have no known competing financial interests or personal relationships that could have appeared to influence the work reported in this paper.

Acknowledgments

The study was supported by the National Natural Science Foundation of China (No. 21807049, 81803430, and 81830052), the Fundamental Research Funds for the Central Universities (JUSRP51703A), the Postgraduate Research & Practice Innovation Program of Jiangsu Province (KYCX19_1888), the Top-notch Academic Programs Project of Jiangsu Higher Education Institutions (PPZY2015B146), the Construction Project of Shanghai Key Laboratory of Molecular Imaging (18DZ2260400), and the Shanghai Municipal Education Commission (Class II Plateau Disciplinary

Construction Program of Medical Technology of SUMHS, 2018–2020).

Appendix A. Supplementary material

Supplementary data to this article can be found online at <https://doi.org/10.1016/j.jare.2021.04.007>.

References

- [1] Zhu J, Hou T, Mao X. Discovery of selective phosphatidylinositol 3-kinase inhibitors to treat hematological malignancies. *Drug Discov Today* 2015;20:988–94. doi: <https://doi.org/10.1016/j.drudis.2015.03.009>.
- [2] Wymann MP, Pirola L. Structure and function of phosphoinositide 3-kinases. *Biochim Biophys Acta* 1998;1436:127–50. doi: [https://doi.org/10.1016/s0005-2760\(98\)00139-8](https://doi.org/10.1016/s0005-2760(98)00139-8).
- [3] Wei M, Wang X, Song Z, Jiao M, Ding J, Meng LH, et al. Targeting PI3Kdelta: emerging therapy for chronic lymphocytic leukemia and beyond. *Med Res Rev* 2015;35:720–52. doi: <https://doi.org/10.1002/med.21341>.
- [4] Zhu J, Wang M, Cao B, Hou T, Mao X. Targeting the phosphatidylinositol 3-kinase/AKT pathway for the treatment of multiple myeloma. *Curr Med Chem* 2014;21:3173–87. doi: <https://doi.org/10.2174/0929867321666140601204513>.
- [5] Garcia-Echeverria C, Sellers WR. Drug discovery approaches targeting the PI3K/Akt pathway in cancer. *Oncogene* 2008;27:5511–26. doi: <https://doi.org/10.1038/onc.2008.246>.
- [6] Hamada K, Sasaki T, Koni PA, Natsui M, Kishimoto H, Sasaki J, et al. The PTEN/PI3K pathway governs normal vascular development and tumor angiogenesis. *Genes Dev* 2005;19:2054–65. doi: <https://doi.org/10.1101/gad.1308805>.
- [7] Vanhaesebroeck B, Leever SJ, Panayotou G, Waterfield MD. Phosphoinositide 3-kinases: A conserved family of signal transducers. *Trends Biochem Sci* 1997;22:267. doi: [https://doi.org/10.1016/s0968-0004\(97\)01061-x](https://doi.org/10.1016/s0968-0004(97)01061-x).
- [8] Krugmann S, Hawkins PT, Pryer N, Braselmann S. Characterizing the interactions between the two subunits of the p101/p110gamma phosphoinositide 3-kinase and their role in the activation of this enzyme by G beta gamma subunits. *J Biol Chem* 1999;274:17152–8. doi: <https://doi.org/10.1074/jbc.274.24.17152>.
- [9] Vanhaesebroeck B, Guillermet-Guibert J, Graupera M, Bilanges B. The emerging mechanisms of isoform-specific PI3K signalling. *Nat Rev Mol Cell Bio* 2010;11:329–41. doi: <https://doi.org/10.1038/nrm2882>.
- [10] Hawkins PT, Anderson KE, Davidson K, Stephens LR. Signalling through class I PI3Ks in mammalian cells. *Biochem Soc Trans* 2006;34:647–62. doi: <https://doi.org/10.1042/BST0340647>.
- [11] Markman B, Dienstmann R, Tabernero J. Targeting the PI3K/Akt/mTOR pathway—beyond rapalogs. *Oncotarget* 2010;1:530–43. doi: <https://doi.org/10.18632/oncotarget.10102>.
- [12] Ito K, Caramori G, Adcock IM. Therapeutic potential of phosphatidylinositol 3-kinase inhibitors in inflammatory respiratory disease. *J Pharmacol Exp Ther* 2007;321:1–8. doi: <https://doi.org/10.1124/jpet.106.111674>.
- [13] Ali AY, Wu X, Eissa N, Hou S, Ghia JE, Murooka TT, et al. Distinct roles for phosphoinositide 3-kinases gamma and delta in malignant B cell migration. *Leukemia* 2018;32:1958–69. doi: <https://doi.org/10.1038/s41375-018-0012-5>.
- [14] Lannutti BJ, Meadows SA, Herman SE, Kashishian A, Steiner B, Johnson AJ, et al. CAL-101, a p110delta selective phosphatidylinositol-3-kinase inhibitor for the treatment of B-cell malignancies, inhibits PI3K signaling and cellular viability. *Blood* 2011;117:591–4. doi: <https://doi.org/10.1182/blood-2010-03-275305>.
- [15] Castillo JJ, Furman M, Winer ES. CAL-101: a phosphatidylinositol-3-kinase p110-delta inhibitor for the treatment of lymphoid malignancies. *Expert Opin Investig Drugs* 2012;21:15–22. doi: <https://doi.org/10.1517/13543784.2012.640318>.
- [16] Markham A. Copanlisib: First Global Approval. *Drugs* 2017;77:1–6. doi: <https://doi.org/10.1007/s40265-017-0838-6>.
- [17] Blair HA. Duvelisib: First Global Approval. *Drugs* 2018;78:1847–53. doi: <https://doi.org/10.1007/s40265-018-1013-4>.
- [18] Ando Y, Iwasa S, Takahashi S, Saka H, Kakizume T, Natsume K, et al. Phase I study of alpelisib (BYL719), an α -specific PI3K inhibitor Japanese patients with advanced solid tumors. *Cancer Sci* 2019;110:1021–31. doi: <https://doi.org/10.1111/cas.13923>.
- [19] Mayer IA, Abramson VG, Formisano L, Balko JM, Estrada MV, Sanders ME, et al. A Phase Ib Study of Alpelisib (BYL719), a PI3Kalpha-Specific Inhibitor, with Letrozole in ER+/HER2- Metastatic Breast Cancer. *Clin Cancer Res* 2017;23:26–34. doi: <https://doi.org/10.1158/1078-0432.CCR-16-0134>.
- [20] Cushing TD, Metz DP, Whittington DA, McGee LR. PI3Kdelta and PI3Kgamma as targets for autoimmune and inflammatory diseases. *J Med Chem* 2012;55:8559–81. doi: <https://doi.org/10.1021/jm300847v>.
- [21] Maxwell MJ, Tsantikos E, Kong AM, Vanhaesebroeck B, Tarlinton DM, Hibbs ML. Attenuation of phosphoinositide 3-kinase delta signaling restrains autoimmune disease. *J Autoimmun* 2012;38:381–91. doi: <https://doi.org/10.1016/j.jaut.2012.04.001>.
- [22] Camps M, Ruckle T, Ji H, Ardisson V, Rintelen F, Shaw J, et al. Blockade of PI3Kgamma suppresses joint inflammation and damage in mouse models of

- rheumatoid arthritis. *Nat Med* 2005;11:936–43. doi: <https://doi.org/10.1038/nm1284>.
- [23] Barber DF, Bartolome A, Hernandez C, Flores JM, Redondo C, Fernandez-Arias C, et al. PI3Kgamma inhibition blocks glomerulonephritis and extends lifespan in a mouse model of systemic lupus. *Nat Med* 2005;11:933–5. doi: <https://doi.org/10.1038/nm1291>.
- [24] Ruckle T, Schwarz MK, Rommel C. PI3Kgamma inhibition: towards an 'aspirin of the 21st century?'. *Nat Rev Drug Discov* 2006;5:903–18. doi: <https://doi.org/10.1038/nrd2145>.
- [25] Pomel V, Klicic J, Covini D, Church DD, Shaw JP, Roulin K, et al. Furan-2-ylmethylene thiazolidinediones as novel, potent, and selective inhibitors of phosphoinositide 3-kinase gamma. *J Med Chem* 2006;49:3857–71. doi: <https://doi.org/10.1021/jm0601598>.
- [26] Bell K, Sunose M, Ellard K, Cansfield A, Taylor J, Miller W, et al. SAR studies around a series of triazolopyridines as potent and selective PI3Kgamma inhibitors. *Bioorg Med Chem Lett* 2012;22:5257–63. doi: <https://doi.org/10.1016/j.bmcl.2012.06.049>.
- [27] Zhu J, Li K, Yu L, Chen Y, Cai Y, Jin J, et al. Targeting phosphatidylinositol 3-kinase gamma (PI3Kgamma): Discovery and development of its selective inhibitors. *Med Res Rev* 2020. doi: <https://doi.org/10.1002/med.21770>.
- [28] Tang J, Zhu J, Yu Y, Zhang Z, Chen G, Zhou X, et al. A virtual screen identified C96 as a novel inhibitor of phosphatidylinositol 3-kinase that displays potent preclinical activity against multiple myeloma in vitro and in vivo. *Oncotarget* 2014;5:3836–48. doi: <https://doi.org/10.18632/oncotarget.1657>.
- [29] Zhu J, Wang M, Yu Y, Qi H, Han K, Tang J, et al. A novel PI3K inhibitor PIK-C98 displays potent preclinical activity against multiple myeloma. *Oncotarget* 2015;6:185–95. doi: <https://doi.org/10.18632/oncotarget.2688>.
- [30] Taha MO, Al-Sha'er MA, Khanfar MA, Al-Nadaf AH. Discovery of nanomolar phosphoinositide 3-kinase gamma (PI3Kgamma) inhibitors using ligand-based modeling and virtual screening followed by in vitro analysis. *Eur J Med Chem* 2014;84:454–65. doi: <https://doi.org/10.1016/j.ejmech.2014.07.056>.
- [31] Berman HM, Westbrook J, Feng Z, Gilliland G, Bhat TN, Weissig H, et al. The Protein Data Bank. *Nucleic Acids Res* 2000;28:235–42. doi: <https://doi.org/10.1093/nar/28.1.235>.
- [32] Kaminski GA, Friesner RA, Tirado-Rives J, Jorgensen WL. Evaluation and Reparametrization of the OPLS-AA Force Field for Proteins via Comparison with Accurate Quantum Chemical Calculations on Peptides. *J Phys Chem B* 2001;105:6474–87. doi: <https://doi.org/10.1021/jp003919d>.
- [33] Tian S, Sun H, Pan P, Li D, Zhen X, Li Y, et al. Assessing an ensemble docking-based virtual screening strategy for kinase targets by considering protein flexibility. *J Chem Inf Model* 2014;54:2664–79. doi: <https://doi.org/10.1021/ci500414b>.
- [34] Wang Z, Sun H, Yao X, Li D, Xu L, Li Y, et al. Comprehensive evaluation of ten docking programs on a diverse set of protein-ligand complexes: the prediction accuracy of sampling power and scoring power. *Phys Chem Chem Phys* 2016;18:12964–75. doi: <https://doi.org/10.1039/c6cp01555g>.
- [35] Gilson MK, Liu T, Baitaluk M, Nicola G, Hwang L, Chong J, et al. A public database for medicinal chemistry, computational chemistry and systems pharmacology. *Nucleic Acids Res* 2015;44(2016):D1045–53. doi: <https://doi.org/10.1093/nar/gkv1072>.
- [36] Shen C, Wang Z, Yao X, Li Y, Lei T, Wang E, et al. Comprehensive assessment of nine docking programs on type II kinase inhibitors: prediction accuracy of sampling power, scoring power and screening power. *Brief Bioinform* 2020;21:282–97. doi: <https://doi.org/10.1093/bib/bbv103>.
- [37] Lipinski CA. Lead- and drug-like compounds: the rule-of-five revolution. *Drug Discov Today Technol* 2004;1:337–41. doi: <https://doi.org/10.1016/j.ddtec.2004.11.007>.
- [38] Walters WP, Stahl MT, Murcko MA. Virtual screening—an overview. *Drug Discov Today* 1998;3:160–78. doi: [https://doi.org/10.1016/S1359-6446\(97\)01163-X](https://doi.org/10.1016/S1359-6446(97)01163-X).
- [39] Zhu J, Ke K, Xu L, Jin J. Discovery of a novel phosphoinositide 3-kinase gamma (PI3Kγ) inhibitor against hematologic malignancies and theoretical studies on its PI3Kγ-specific binding mechanisms. *RSC Adv* 2019;9:20207–15. doi: <https://doi.org/10.1039/C9RA02649E>.
- [40] Li K, Zhu J, Xu L, Jin J. Rational Design of Novel Phosphoinositide 3-Kinase Gamma (PI3Kgamma) Selective Inhibitors: A Computational Investigation Integrating 3D-QSAR, Molecular Docking and Molecular Dynamics Simulation. *Chem Biodivers* 2019;16. doi: <https://doi.org/10.1002/cbdv.201900105e1900105>.
- [41] Yang JJ, Ursu O, Lipinski CA, Sklar LA, Oprea TI, Bologa CG. Badapple: promiscuity patterns from noisy evidence. *J Cheminform* 2016;8:29. doi: <https://doi.org/10.1186/s13321-016-0137-3>.
- [42] Stork C, Chen Y, Šicho M, Kirchmair J. Hit Dexter 2.0: Machine-Learning Models for the Prediction of Frequent Hitters. *J Chem Inf Model* 2019;59:1030–43. doi: <https://doi.org/10.1021/acs.jcim.8b00677>.
- [43] Williams O, Houseman BT, Kunkel EJ, Aizenstein B, Hoffman R, Knight ZA, et al. Discovery of dual inhibitors of the immune cell PI3Ks p110delta and p110gamma: a prototype for new anti-inflammatory drugs. *Chem Biol* 2010;17:123–34. doi: <https://doi.org/10.1016/j.chembiol.2010.01.010>.
- [44] Fradera X, Methot JL, Achab A, Christopher M, Altman MD, Zhou H, et al. Design of selective PI3Kδ inhibitors using an iterative scaffold-hopping workflow. *Bioorg Med Chem Lett* 2019;29:2575–80. doi: <https://doi.org/10.1016/j.bmcl.2019.08.004>.
- [45] Zhang X, Vadas O, Perisic O, Anderson KE, Clark J, Hawkins PT, et al. Structure of lipid kinase p110β/p85β elucidates an unusual SH2-domain-mediated inhibitory mechanism. *Mol Cell* 2011;41:567–78. doi: <https://doi.org/10.1016/j.molcel.2011.01.026>.
- [46] Leahy JW, Buhr CA, Johnson HW, Kim BG, Baik T, Cannon J, et al. Discovery of a novel series of potent and orally bioavailable phosphoinositide 3-kinase gamma inhibitors. *J Med Chem* 2012;55:5467–82. doi: <https://doi.org/10.1021/jm300403a>.
- [47] Liang C, Li Y, Luo J. A Novel Method to Detect Functional microRNA Regulatory Modules by Bicliques Merging. *IEEE/ACM Trans Comput Biol Bioinform* 2016;13:549–56. doi: <https://doi.org/10.1109/TCBB.2015.2462370>.
- [48] Martyna GJ. Remarks on "Constant-temperature molecular dynamics with momentum conservation". *Phys Rev E Stat Phys Plasmas Fluids Relat Interdiscip Topics* 1994;50:3234–6. doi: <https://doi.org/10.1103/physreve.50.3234>.
- [49] Evans DJ, Holian BL. The Nose-Hoover thermostat. *J Chem Phys* 1985;83:4069–74. doi: <https://doi.org/10.1063/1.449071>.
- [50] Darden T, York D, Pedersen L. Particle mesh Ewald: An N-log(N) method for Ewald sums in large systems. *J Chem Phys* 1993;98:10089–92. doi: <https://doi.org/10.1063/1.464397>.
- [51] Singh PK, Silakari O. Molecular dynamics guided development of indole based dual inhibitors of EGFR (T790M) and c-MET. *Bioorg Chem* 2018;79:163–70. doi: <https://doi.org/10.1016/j.bioorg.2018.04.001>.
- [52] Apse B, Blair JA, Gonzalez B, Nazif TM, Feldman ME, Aizenstein B, et al. Targeted polypharmacology: discovery of dual inhibitors of tyrosine and phosphoinositide kinases. *Nat Chem Biol* 2008;4:691–9. doi: <https://doi.org/10.1038/nchembio.117>.
- [53] Folkes AJ, Ahmadi K, Alderton WK, Alix S, Baker SJ, Box G, et al. The identification of 2-(1H-indazol-4-yl)-6-(4-methanesulfonyl-piperazin-1-ylmethyl)-4-morpholin-4-yl-t hieno[3,2-d]pyrimidine (GDC-0941) as a potent, selective, orally bioavailable inhibitor of class I PI3 kinase for the treatment of cancer. *J Med Chem* 2008;51:5522–32. doi: <https://doi.org/10.1021/jm800295d>.
- [54] Cheng H, Li C, Bailey S, Baxi SM, Goulet L, Guo L, et al. Discovery of the Highly Potent PI3K/mTOR Dual Inhibitor PF-04979064 through Structure-Based Drug Design. *ACS Med Chem Lett* 2013;4:91–7. doi: <https://doi.org/10.1021/ml300309h>.
- [55] Staben ST, Siu M, Goldsmith R, Olivero AG, Do S, Burdick DJ, et al. Structure-based design of thienobenzoxepin inhibitors of PI3-kinase. *Bioorg Med Chem Lett* 2011;21:4054–8. doi: <https://doi.org/10.1016/j.bmcl.2011.04.124>.
- [56] Gonzalez-Lopez de Turiso F, Shin Y, Brown M, Cardozo M, Chen Y, Fong D, et al. Discovery and in vivo evaluation of dual PI3Kβ/δ inhibitors. *J Med Chem* 2012;55:7667–85. doi: <https://doi.org/10.1021/jm300679u>.
- [57] Norman MH, Andrews KL, Bo YY, Booker SK, Caenepel S, Cee VJ, et al. Selective class I phosphoinositide 3-kinase inhibitors: optimization of a series of pyridyltriazines leading to the identification of a clinical candidate, AMG 511. *J Med Chem* 2012;55:7796–816. doi: <https://doi.org/10.1021/jm300846z>.
- [58] Collier PN, Martinez-Botella G, Cornebise M, Cottrell KM, Doran JD, Griffith JP, et al. Structural basis for isoform selectivity in a class of benzothiazole inhibitors of phosphoinositide 3-kinase gamma. *J Med Chem* 2015;58:517–21. doi: <https://doi.org/10.1021/jm500362j>.
- [59] Cushing TD, Hao X, Shin Y, Andrews K, Brown M, Cardozo M, et al. Discovery and in vivo evaluation of (S)-N-(1-(7-fluoro-2-(pyridin-2-yl)quinolin-3-yl)ethyl)-9H-purin-6-amine (AMG319) and related PI3Kδ inhibitors for inflammation and autoimmune disease. *J Med Chem* 2015;58:480–511. doi: <https://doi.org/10.1021/jm501624r>.
- [60] Scott WJ, Hentemann MF, Rowley RB, Bull CO, Jenkins S, Bullion AM, et al. Discovery and SAR of Novel 2,3-Dihydroimidazo[1,2-c]quinazoline PI3K Inhibitors: Identification of Copanlisib (BAY 80-6946). *ChemMedChem* 2016;11:1517–30. doi: <https://doi.org/10.1002/cmdc.201600148>.